 CMES, vol.8, no.3, pp.177-190, 2005

On Three-Dimensional Fracture Mechanics Analysis by an Enriched Meshless Method

Wen-Hwa Chen[1] and Cheng-Hung Chen[2]

Abstract: An enriched meshless method, using meshless interpolations and a global Galerkin approach, is developed for the analysis of three-dimensional fracture problems. The displacement field which accounts for the stress singularity nearby the crack front and the boundary layer effect at the intersection between the crack front and the free surface of the structure is adopted to enrich the trial functions. The three-dimensional stress intensity factors can thus be treated as independent unknown parameters and calculated with the nodal displacements directly. To estimate the accuracy of the method developed, several representative three-dimensional cracks are analyzed. These include single-edge crack, embedded elliptical and semi-elliptical surface cracks, and quarter-elliptical corner crack, etc. The variation of the three-dimensional stress intensity factors along the crack front is drawn in details. The influence of crack sizes and boundary layer effect on the three-dimensional stress intensity factors is also studied. Excellent agreements between the calculated results and those available in the literature demonstrate the high accuracy and applicability of the method developed.

keyword: Meshless Method, Fracture Mechanics Analysis, Boundary Layer Effect, Stress Intensity Factors

1 Introduction

Many numerical methods have been developed to deal with practical fracture mechanics problems with irregular geometries and complicated boundary conditions. Among these methods, the finite element method is extensively applied popularly (Atluri et al., 1975; 1979; Barsoum, 1976; Chen et al., 1984). Another useful method, developed extensively for 3-D non-planar crack growth under fatigue, is the Schwartz-Neumann alternating method (see, for instance, Han et al., 2002; Atluri, 2005).

The meshless method has been recently studied to overcome some of the shortcomings of the finite element method, such as the labor intensive process of mesh generation in complex 3-D structures. It does not require a mesh because the trial functions are derived based on a moving least square (MLS) approximation method or a variety of other meshless approximations of trial functions (Atluri, 2004a; Han et al., 2004). The meshless local Petrov-Galerkin (MLPG) method (Kim et al., 2000; Lin et al., 2000; Ching et al., 2001; Atluri et al., 2002; 2003; 2004a, b; 2005; Han et al., 2002; 2004; Li et al., 2003) and the element-free Galerkin method (EFGM) (Belytschko et al., 1994; Liu et al., 1994; Chen et al., 2001) are two of the most well-knowns. The MLPG method is a union of local weak form and does not need to construct cells for numerical integration, and it is considered as a truly meshless method. In the MLPG finite volume mixed method (Atluri et al., 2004b), the local weak form is shown to be computable in a very simple way, by performing integrations only over the surface of each overlapping cell. As for EFGM, however, since it is based on a global weak form, the equilibrium within the global domain is satisfied approximately. Hence, after constructing a grid of background cells, stable numerical calculation can be achieved through the integrations over each background cell. The EFGM method is adopted in this work.

By applying the EFGM to analyze the cracked structure, different distribution of nodal densities in the vicinity of the crack front, in general, will affect the determination of stress intensity factors (Organ et al., 1996; Fleming et al., 1997). Fleming et al. (1997) employed enriched trial functions and basis functions to analyze two-dimensional fracture problems. By his approach, how-

[1] Tsing Hua Professor of Engineering, corresponding author, Department of Power Mechanical Engineering, National Tsing Hua University, Hsinchu, Taiwan 30043, Republic of China E-mail : whchen@pme.nthu.edu.tw

[2] Graduate student

ever, the calculation of the enriched basis functions will not only encounter ill-conditioning but also increase the dimension of the calculated matrix, especially in analyzing the three-dimensional fracture problems (Sukumar et al., 1997). In addition, by the enriched trial functions as used in Fleming et al. (1997), the modified nodal coefficients need be first determined to specify the displacement field.

The objective of this work is therefore to present an enriched element-free Galerkin method which can be employed to analyze three-dimensional fracture problems efficiently and accurately. The trial functions are enriched with the displacement field which accounts for the stress singularity nearby the crack front. The boundary layer stress singularity (Folias, 1975) at the intersection between the crack front and free surface of the cracked structure is also embedded. The three-dimensional stress intensity factors and nodal displacements can be calculated directly. Excellent agreements between the present computed results and the referenced solutions are drawn.

2 Formulation of Enriched Element-Free Galerkin Method

As depicted in Fig. 1, a three-dimensional linear elastic structure Ω is enclosed by a surface boundary Γ. Ω includes an enriched domain Ω_s surrounding the crack front and a regular domain Ω_r. The singular stress field (Williams, 1957) in the enriched domain Ω_s nearby the crack front is noted.

According to the principle of minimum total potential energy (Fung, 1965), when this elastic conservative system is in stable equilibrium, the total potential energy Π of the structure Ω is found as

$$\Pi = U - W = \min.,$$

where U represents the strain energy of the system and W is the work done by the external forces. U and W can be respectively written as

$$U = \frac{1}{2}\int_{\Omega_r+\Omega_s} \{\varepsilon\}^T [E] \{\varepsilon\} d\Omega$$

and

$$W = \int_{\Omega_r+\Omega_s} \{u\}^{\mathrm{T}} \left\{\overline{F}\right\} d\Omega + \int_{\Gamma_{tr}+\Gamma_{ts}} \{u\}^{\mathrm{T}} \left\{\overline{T}\right\} d\Gamma,$$

where $\{u\}$ is the displacement vector, $\{\varepsilon\}$ is the strain tensor, $[E]$ is the matrix of the material constants, $\{\overline{F}\}$ is the body force vector, and $\left\{\overline{T}\right\}$ is the prescribed surface traction vector that acts on the boundaries Γ_{tr} and Γ_{ts}. Γ_{ts} represents the surface traction boundary in the enriched domain Ω_s near the crack front and Γ_{tr} denotes the surface traction boundary in the regular domain Ω_r. Accordingly, the total potential energy Π can be written as

$$\begin{aligned}\Pi = &\int_{\Omega_r+\Omega_s} \left(\frac{1}{2}\{\varepsilon\}^T [E] \{\varepsilon\} - \{u\}^{\mathrm{T}} \left\{\overline{F}\right\}\right) d\Omega \\ &- \int_{\Gamma_{tr}+\Gamma_{ts}} \{u\}^{\mathrm{T}} \left\{\overline{T}\right\} d\Gamma\end{aligned} \tag{1}$$

Since the trial functions of the enriched EFGM are derived by applying the MLS approximation method, the trial functions between any node i in the structure and any node j on the boundary do not satisfy the Kronecker delta property for satisfying the displacement boundary conditions (Belytschko et al., 1994). The penalty method (Zhu et al., 1998) is therefore adopted herein to improve the boundary conditions. After the prescribed displacement boundary conditions are determined by the penalty method, the total potential energy Π in Eqn (1) can be modified as Π^*, say,

$$\begin{aligned}\Pi^* = &\int_{\Omega_r+\Omega_s} \left(\frac{1}{2}\{\varepsilon\}^T [E] \{\varepsilon\} - \{u\}^{\mathrm{T}} \left\{\overline{F}\right\}\right) d\Omega \\ &- \int_{\Gamma_{tr}+\Gamma_{ts}} \{u\}^{\mathrm{T}} \left\{\overline{T}\right\} d\Gamma \\ &+ \frac{\alpha}{2}\int_{\Gamma_{ur}+\Gamma_{us}} (\{u\}-\{\overline{u}\})^T (\{u\}-\{\overline{u}\}) d\Gamma \\ &= \min.\end{aligned} \tag{2}$$

where $\{\overline{u}\}$ is the prescribed displacement vector on the boundaries Γ_{ur} and Γ_{us}. Γ_{ur} is the prescribed displacement boundary in the regular domain, and Γ_{us} represents the prescribed displacement boundary in the enriched domain Ω_s nearby the crack front.

If the displacement boundary conditions are satisfied, that is $\{u\}-\{\overline{u}\} = \{0\}$ on the boundary $\Gamma_{ur}+\Gamma_{us}$, $\Pi^* = \Pi$ and no penalty energy needs to be added to the total potential energy Π. In contrast, if $\{u\}-\{\overline{u}\} \neq \{0\}$ on the boundary $\Gamma_{ur}+\Gamma_{us}$, the displacement boundary condition can be satisfied through the compensation of the given penalty energy with parameter α.

The displacement field of any point in the regular domain Ω_r and the enriched domain Ω_s can be interpolated by considering the vector of nodal displacements $\{q\}$ of all

nodes in the structure:

$$\{u\} = [\Phi]\{q\} \quad \text{in} \quad \Omega_r \tag{3}$$

and

$$\{u\} = [\Phi]\{q\} + [\Psi]\{K\} \quad \text{in} \quad \Omega_s, \tag{4}$$

where $[\Phi]$ and $[\Psi]$ are the trial function matrix for the displacement field in the regular domain Ω_r and enriched domain Ω_s. $\{K\}$ represents the vector of three-dimensional stress intensity factors for all nodes on the crack front in the enriched domain Ω_s. The derivation of the trial function matrix $[\Phi]$ and $[\Psi]$ will be discussed in the next section.

The strain–displacement relationship yields

$$\{\varepsilon\} = [B_r]\{q\} \quad \text{in} \quad \Omega_r \tag{5}$$

and

$$\{\varepsilon\} = [B_r]\{q\} + [B_s]\{K\} \quad \text{in} \quad \Omega_s. \tag{6}$$

Substituting Eqns (3)$\sim$(6) into Eqn (2), the modified total potential energy Π^* can be rewritten as

$$\begin{aligned}
\Pi^* = & \frac{1}{2}\int_{\Omega_r} \{q\}^T [B_r]^{\mathrm{T}} [E] [B_r]\{q\}\, d\Omega \\
& - \int_{\Omega_r} ([\Phi]\{q\})^T \left\{\overline{F}\right\} d\Omega \\
& - \int_{\Gamma_{tr}} ([\Phi]\{q\})^T \left\{\overline{T}\right\} d\Gamma \\
& + \frac{\alpha}{2}\int_{\Gamma_{ur}} ([\Phi]\{q\} - \{\overline{u}\})^T ([\Phi]\{q\} - \{\overline{u}\})\, d\Gamma \\
& + \frac{1}{2}\int_{\Omega_s} ([B_r]\{q\} + [B_s]\{K\})^T [E] \\
& \qquad ([B_r]\{q\} + [B_s]\{K\})\, d\Omega \\
& - \int_{\Omega_s} ([\Phi]\{q\} + [\Psi]\{K\})^T \left\{\overline{F}\right\} d\Omega \\
& - \int_{\Gamma_{ts}} ([\Phi]\{q\} + [\Psi]\{K\})^T \left\{\overline{T}\right\} d\Gamma \\
& + \frac{\alpha}{2}\int_{\Gamma_{us}} ([\Phi]\{q\} + [\Psi]\{K\} - \{\overline{u}\})^T \\
& \qquad ([\Phi]\{q\} + [\Psi]\{K\} - \{\overline{u}\})\, d\Gamma \\
& = \min.
\end{aligned} \tag{7}$$

Since the strain energy is positive-definite, the modified total potential energy Π^* given by Eqn (7) becomes minimum when the system is stationary. The stationary conditions of Π^* with respect to $\{q\}^T$ and $\{K\}^T$ are

$$\frac{\partial \Pi^*}{\partial \{q\}^T} = \frac{\partial \Pi^*}{\partial \{K\}^T} = \{0\}.$$

That is

$$\begin{aligned}
& \begin{bmatrix} [K_r] + [K_r^*] & [K_{rs}] + [K_{rs}^*] \\ [K_{sr}] + [K_{sr}^*] & [K_s] + [K_s^*] \end{bmatrix} \begin{Bmatrix} \{q\} \\ \{K\} \end{Bmatrix} \\
& \quad = \begin{Bmatrix} \{Q_r\} + \{Q_r^*\} \\ \{Q_s\} + \{Q_s^*\} \end{Bmatrix},
\end{aligned} \tag{8}$$

where

$$[K_r] = \int_{\Omega_r+\Omega_s} [B_r]^T [E] [B_r]\, d\Omega,$$

$$[K_{rs}] = \int_{\Omega_s} [B_r]^T [E] [B_s]\, d\Omega,$$

$$[K_{sr}] = \int_{\Omega_s} [B_s]^T [E] [B_r]\, d\Omega,$$

$$[K_s] = \int_{\Omega_s} [B_s]^T [E] [B_s]\, d\Omega,$$

$$\{Q_r\} = \int_{\Omega_r+\Omega_s} [\Phi]^T \left\{\overline{F}\right\} d\Omega + \int_{\Gamma_{tr}+\Gamma_{ts}} [\Phi]^T \left\{\overline{T}\right\} d\Gamma,$$

$$\{Q_s\} = \int_{\Omega_s} [\Psi]^T \left\{\overline{F}\right\} d\Omega + \int_{\Gamma_{ts}} [\Psi]^T \left\{\overline{T}\right\} d\Gamma,$$

$$[K_r^*] = \alpha \int_{\Gamma_{ur}+\Gamma_{us}} [\Phi]^T [S] [\Phi]\, d\Gamma,$$

$$[K_{rs}^*] = \alpha \int_{\Gamma_{us}} [\Phi]^T [S] [\Psi]\, d\Gamma,$$

$$[K_{sr}^*] = \alpha \int_{\Gamma_{us}} [\Psi]^T [S] [\Phi]\, d\Gamma,$$

$$[K_s^*] = \alpha \int_{\Gamma_{us}} [\Psi]^T [S] [\Psi]\, d\Gamma,$$

$$\{Q_r^*\} = \alpha \int_{\Gamma_{ur}+\Gamma_{us}} [\Phi]^T [S] \{\overline{u}\}\, d\Gamma,$$

$$\{Q_s^*\} = \alpha \int_{\Gamma_{us}} [\Phi]^T [S] \{\overline{u}\}\, d\Gamma,$$

and

$$[S] = \begin{bmatrix} S_1 & 0 & 0 \\ 0 & S_2 & 0 \\ 0 & 0 & S_3 \end{bmatrix}.$$

S_1, S_2 and S_3 represent the indicator of prescribed displacement boundary conditions on the boundary Γ_{ur} or Γ_{us} in x, y and z directions, respectively. Thus, they can be assigned as either 1 or 0.

For a three-dimensional cracked structure, once the load vectors $\{Q_r\} + \{Q_r^*\}$ and $\{Q_s\} + \{Q_s^*\}$ are known, the vector of nodal displacements $\{q\}$ of the entire structure

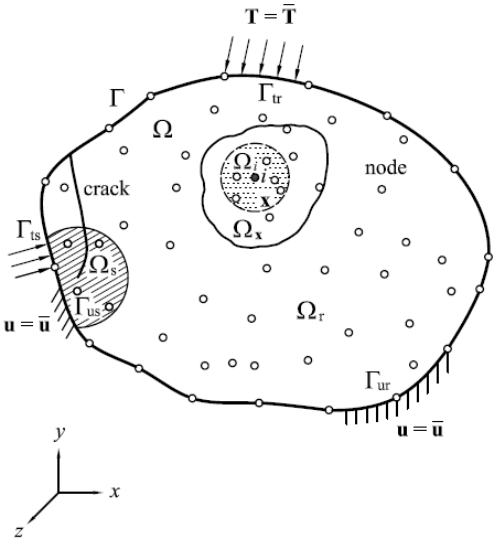

Figure 1 : The meshless model of the structure with a crack

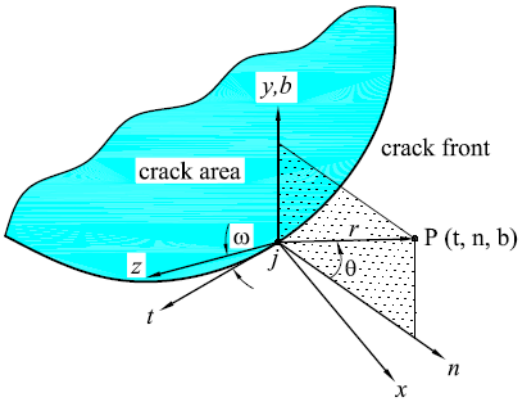

Figure 2 : The local polar coordinates of the node ***j*** on the crack front

and the vector of three-dimensional stress intensity factors $\{K\}$ of the nodes on the crack front can be computed from Eqn (8) subjected to the prescribed displacement boundary conditions. If the structure contains no crack, the enriched domain Ω_s vanishes and Eqn (8) is reduced to

$$([K_r]+[K_r^*])\{q\}=\{Q_r\}+\{Q_r^*\}.$$

3 Enriched Trial Functions

As indicated in Fig. 1, if the material point $\boldsymbol{x}$ is located in the enriched domain Ω_s, the displacement components $u^\alpha(\boldsymbol{x})(\alpha=1,2,3)$ of $\boldsymbol{x}$ can be derived as

$$u^\alpha(\boldsymbol{x})=\sum_{i=1}^{m}p_i(\boldsymbol{x})a_i^\alpha(\boldsymbol{x})+\sum_{j=1}^{n_c}\sum_{k=\mathrm{I}}^{\mathrm{III}}h_{kj}^\alpha(\boldsymbol{x})k_j^k, \tag{9}$$

where $p_i(\boldsymbol{x})$ is a complete monomial basis of order m and $a_i^\alpha(\boldsymbol{x})$ denotes the undetermined coefficients. $h_{kj}^\alpha(\boldsymbol{x})$ represents the basis function for the displacement field of the n_c nodes on the crack front. The suffix j denotes the correspondence with node j on the crack front and $k(k=\mathrm{I},\mathrm{II},\mathrm{III})$ specifies the modes of cracks, *i.e.*

$$h_{kj}^\alpha(\boldsymbol{x})=\sum_{\beta=\mathrm{I}}^{\mathrm{III}}t_{\beta j}^\alpha d_{kj}^\beta,$$

where $t_{\beta j}^\alpha$ and d_{kj}^β are the relationship terms between the global coordinates $x-y-z$ and the t-axis of the local coordinates $t-n-b$ (see Appendix A). If $\boldsymbol{x}$ is in the regular domain Ω_r, the second term on the right-hand side of Eqn (9) will vanish. Eqn (9) can be written in matrix form as

$$u^\alpha(\boldsymbol{x})=\{p(\boldsymbol{x})\}^T\{a^\alpha(\boldsymbol{x})\}+\{h^\alpha(\boldsymbol{x})\}^T\{K\}, \tag{10}$$

where

$$\{h^\alpha(\boldsymbol{x})\}^T=\begin{bmatrix} h_{\mathrm{I}1}^\alpha(\boldsymbol{x}) & h_{\mathrm{II}1}^\alpha(\boldsymbol{x}) & h_{\mathrm{III}1}^\alpha(\boldsymbol{x}) & \cdots \\ h_{\mathrm{I}n_c}^\alpha(\boldsymbol{x}) & h_{\mathrm{II}n_c}^\alpha(\boldsymbol{x}) & h_{\mathrm{III}n_c}^\alpha(\boldsymbol{x}) & \end{bmatrix}_{1\times 3n_c}$$

and

$$\{K\}^T=\begin{bmatrix} k_1^{\mathrm{I}} & k_1^{\mathrm{II}} & k_1^{\mathrm{III}} & \cdots & k_{n_c}^{\mathrm{I}} & k_{n_c}^{\mathrm{II}} & k_{n_c}^{\mathrm{III}} \end{bmatrix}_{1\times 3n_c}.$$

As shown in Fig. 1, each node i in the structure Ω is associated with a support domain Ω_i. The union of the support domains $\Omega_i$of each node i in the vicinity of $\boldsymbol{x}$ constitutes a sub-domain $\Omega_{\boldsymbol{x}}$ in which $\boldsymbol{x}$ has influence.

If $\boldsymbol{x}$ is located in the enriched domain Ω_s, the approximate displacement field in $\Omega_{\boldsymbol{x}}$ will be influenced by the approximate function $\{p(\boldsymbol{x}_i)\}^T\{a^\alpha(\boldsymbol{x})\}+\{h^\alpha(\boldsymbol{x}_i)\}^T\{K\}$ and the nodal displacement components $q_i^\alpha(\alpha=1,2,3)$ of each node i. The difference between the approximate displacement function $\{p(\boldsymbol{x}_i)\}^T\{a^\alpha(\boldsymbol{x})\}+$

$\{h^\alpha(\boldsymbol{x}_i)\}^T\{K\}$ and the nodal displacement components $q_i^\alpha(\alpha=1,2,3)$ can be minimized in a least-square sense with respect to the weight value $w_i(\boldsymbol{x})$ of each node i. Hence, the weighted least square discrete L_2 error norm can be expressed as

$$\begin{aligned}&J\left(\{a^\alpha(\boldsymbol{x})\}\right)\\&=\sum_{i=1}^{n} w_i(\boldsymbol{x})\left(\{p(x_i)\}^T\{a^\alpha(\boldsymbol{x})\}+\{h^\alpha(x_i)\}^T\{K\}-q_i^\alpha\right)^2\\&=\left([P]\{a^\alpha(\boldsymbol{x})\}+[H^\alpha]\{K\}-\{q^\alpha\}\right)^T[W]\\&\quad\left([P]\{a^\alpha(\boldsymbol{x})\}+[H^\alpha]\{K\}-\{q^\alpha\}\right),\end{aligned}$$

where the vector of nodal displacement field $\{q^\alpha\}(\alpha=1,2,3)$ of the n nodes in$\Omega_{\boldsymbol{x}}$ constitutes the vector of nodal displacements $\{q\}$ which can be computed from Eqn (8). That is

$$\{q^\alpha\}^T=\begin{bmatrix} q_1^\alpha & q_1^\alpha & \cdots & q_1^\alpha \end{bmatrix}_{1\times n}.$$

The matrices $[P]$, $[W]$ and $[H^\alpha]$ can be respectively given by

$$[P]=\begin{bmatrix} \{p(\boldsymbol{x}_1)\}^T\\ \{p(\boldsymbol{x}_2)\}^T\\ \vdots\\ \{p(\boldsymbol{x}_n)\}^T\end{bmatrix}_{n\times m},$$

$$[P]=\begin{bmatrix} w_1(\boldsymbol{x}) & 0 & 0 & 0\\ 0 & w_2(\boldsymbol{x}) & 0 & 0\\ 0 & 0 & \ddots & 0\\ 0 & 0 & 0 & w_n(\boldsymbol{x})\end{bmatrix}_{n\times m},$$

and

$$[H^\alpha]=\begin{bmatrix} \{h_\alpha(\boldsymbol{x}_1)\}^T\\ \{h_\alpha(\boldsymbol{x}_2)\}^T\\ \vdots\\ \{h_\alpha(\boldsymbol{x}_n)\}^T\end{bmatrix}_{n\times m}.$$

If $\boldsymbol{x}$ is in the regular domain Ω_r, the function $\{h^\alpha(\boldsymbol{x}_i)\}^T\{K\}$ and the matrix $[H^\alpha]\{K\}$ will disappear.

Since $[W]$ is positive definite, the minimization of the weighted discrete function $J(\{a^\alpha(\boldsymbol{x})\})$ can be obtained by the stationary condition with respect to $\{a^\alpha(\boldsymbol{x})\}$, *i.e.*

$$\frac{\partial J\left(\{a^\alpha(\boldsymbol{x})\}\right)}{\partial\{a^\alpha(\boldsymbol{x})\}^T}=\{0\}.$$

This leads to

$$\left([P]^T[W][P]\right)\{a^\alpha(\boldsymbol{x})\}=\left([P]^T[W]\right)\left(\{q^\alpha\}-[H^\alpha]\{K\}\right).$$

If the inverse of matrix $\left([P]^T[W][P]\right)$ exists, then

$$\begin{aligned}\{a^\alpha(\boldsymbol{x})\}=&\left([P]^T[W][P]\right)^{-1}\\&\left([P]^T[W]\right)\left(\{q^\alpha\}-[H^\alpha]\{K\}\right).\end{aligned}\tag{11}$$

Notably, the nodes in the vicinity of $\boldsymbol{x}$ cannot be co-line or co-plane; otherwise, the rank of $\left([P]^T[W][P]\right)$ would be less than m and its inverse will not exist. Besides, because the vector $\{a^\alpha(\boldsymbol{x})\}$ has m undetermined coefficients, the number of nodes taken in $\Omega_{\boldsymbol{x}}$ can not be less than m, *i.e.* $n\geq m$.

Substituting Eqn (11) into Eqn (10), $u^\alpha(\boldsymbol{x})$ can be expressed as

$$\begin{aligned}u^\alpha(\boldsymbol{x})=&\{p(\boldsymbol{x})\}^T\left([P]^T[W][P]\right)^{-1}\\&\left([P]^T[W]\right)\left(\{q^\alpha\}-[H^\alpha]\{K\}\right)+\{h^\alpha(\boldsymbol{x})\}^T\{K\}\\=&\{p(x)\}^T\left([P]^T[W][P]\right)^{-1}\left([P]^T[W]\right)\{q^\alpha\}\\&+\left(\{h^\alpha(\boldsymbol{x})\}^T-\{p(\boldsymbol{x})\}^T\left([P]^T[W][P]\right)^{-1}\right.\\&\left.\left([P]^T[W]\right)[H^\alpha]\right)\{K\}.\end{aligned}$$

The above displacement components can be rearranged in the vector form $\{u\}$ as

$$\begin{aligned}\{u\}=&\begin{bmatrix} u^1(\boldsymbol{x}) & u^2(\boldsymbol{x}) & u^3(\boldsymbol{x})\end{bmatrix}^T\\=&\begin{bmatrix} \phi_1(\boldsymbol{x}) & 0 & 0 & \cdots\\ 0 & \phi_1(\boldsymbol{x}) & 0 & \cdots\\ 0 & 0 & \phi_1(\boldsymbol{x}) & \cdots\\ \phi_n(\boldsymbol{x}) & 0 & 0 & \\ 0 & \phi_n(\boldsymbol{x}) & 0 & \\ 0 & 0 & \phi_n(\boldsymbol{x}) & \end{bmatrix}\begin{Bmatrix} q_1^1\\ q_1^2\\ q_1^3\\ \vdots\\ q_n^1\\ q_n^2\\ q_n^3\end{Bmatrix}\end{aligned}$$

$$+\begin{bmatrix} \psi_{11}^1(\boldsymbol{x}) & \psi_{21}^1(\boldsymbol{x}) & \psi_{31}^1(\boldsymbol{x}) & \cdots \\ \psi_{11}^2(\boldsymbol{x}) & \psi_{21}^2(\boldsymbol{x}) & \psi_{31}^2(\boldsymbol{x}) & \cdots \\ \psi_{11}^3(\boldsymbol{x}) & \psi_{21}^3(\boldsymbol{x}) & \psi_{31}^3(\boldsymbol{x}) & \cdots \end{bmatrix}$$

$$\begin{bmatrix} \psi_{1n_c}^1(\boldsymbol{x}) & \psi_{2n_c}^1(\boldsymbol{x}) & \psi_{3n_c}^1(\boldsymbol{x}) \\ \psi_{1n_c}^2(\boldsymbol{x}) & \psi_{2n_c}^2(\boldsymbol{x}) & \psi_{3n_c}^2(\boldsymbol{x}) \\ \psi_{1n_c}^3(\boldsymbol{x}) & \psi_{2n_c}^3(\boldsymbol{x}) & \psi_{3n_c}^3(\boldsymbol{x}) \end{bmatrix} \begin{Bmatrix} k_1^{\mathrm{I}} \\ k_1^{\mathrm{II}} \\ k_1^{\mathrm{III}} \\ \vdots \\ k_{n_c}^{\mathrm{I}} \\ k_{n_c}^{\mathrm{II}} \\ k_{n_c}^{\mathrm{III}} \end{Bmatrix}$$

$$= [\Phi]\{q\} + [\Psi]\{K\}.$$

The trial functions $\phi_i(\boldsymbol{x})(i = 1,2,\cdots,n)$ and their enriched parts $\psi_{ij}^{\alpha}(\boldsymbol{x})(i,\alpha = 1,2,3 \text{ and } j = 1,2,\cdots,n_c)$ can be respectively expressed as

$$\phi_i(\boldsymbol{x}) = \sum_{j=1}^{m} p_j(\boldsymbol{x}) \left(\left([P]^T [W] [P] \right)^{-1} \left([P]^T [W] \right) \right)_{ji} \quad (12)$$

and

$$\psi_{ij}^{\alpha}(\boldsymbol{x}) = h_{ij}^{\alpha}(\boldsymbol{x}) - \sum_{k=1}^{m} p_k(\boldsymbol{x}) \left(\left([P]^T [W] [P] \right)^{-1} \left([P]^T [W] \right) [H^{\alpha}] \right)_{kj} \delta_{i\alpha}. \quad (13)$$

4 Calculation Procedure

The EFGM constructs a grid of cells for the structure Ω such that the numerical integration can be performed by the Gauss quadrature. When the structure Ω is appropriately separated into numerous cells Ω_{ci}, each cell Ω_{ci} had better be regular for programming, but the boundaries of the cells need be consistent with the overall geometric boundary. If part of the structure or the crack is in Ω_{ci}, Ω_{ci} can be made to match the geometry (Kaljević et al., 1997). Fig. 3 presents the grid of cells. After all of the cells are assembled in the structure, Eqn (2) can be written as

$$\begin{aligned} \Pi^* = & \sum_{i=1}^{N_c} \int_{\Omega_{ci}} \left(\frac{1}{2} \{\varepsilon\}^T [E] \{\varepsilon\} - \{u\}^{\mathrm{T}} \{\overline{F}\} \right) d\Omega_{ci} \\ & - \sum_{i=1}^{L_1} \int_{\Gamma_{ti}} \{u\}^{\mathrm{T}} \{\overline{T}\} d\Gamma_{ti} \\ & + \sum_{i=1}^{L_2} \frac{\alpha}{2} \int_{\Gamma_{ui}} (\{u\} - \{\overline{u}\})^T (\{u\} - \{\overline{u}\}) d\Gamma_{ui} \\ & = \min., \end{aligned} \quad (14)$$

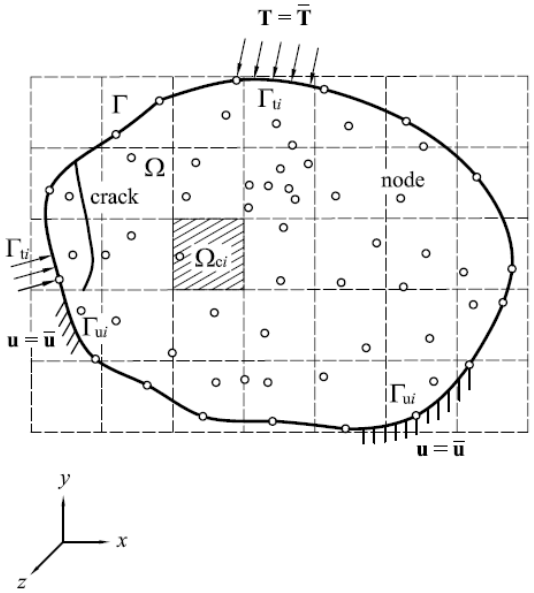

Figure 3 : The divided cells and their boundaries

where N_c is the total number of cells in the structure; L_1 is the number of divided surface traction boundaries Γ_{ti} and L_2 is the number of division of the displacement boundaries Γ_{ui}. By numerical experiments, the penalty parameter α used herein is 10^{12}. This value is within the range $3 \times 10^{10} \sim 3 \times 10^{14}$ as suggested by Zhu et al. (1998). The selected quadrature order n_Q and the number of nodes in the cell n_{cell} should satisfy the relationship $n_Q \geq \sqrt[3]{n_{cell}} + 3$ (Chen et al., 2001).

As for the calculation procedure, firstly the nodes are configured, and the basis function matrix $[P]$ and the weight function matrix $[W]$ are established. After considering the continuity and numerical stability of the trial functions $\phi_i(\boldsymbol{x})$, the spline function is selected as the weight function $w_i(\boldsymbol{x})$ to form the matrix $[W]$ as follows (Atluri et al., 1999)

$$w_i(\boldsymbol{x}) = \begin{cases} 1 - 6(\frac{d_i}{r_i})^2 + 8(\frac{d_i}{r_i})^3 - 3(\frac{d_i}{r_i})^4 & 0 \leq d_i \leq r_i \\ 0 & r_i \leq d_i \end{cases},$$

where $d_i = |\boldsymbol{x} - \boldsymbol{x}_i|$, d_i is the distance between $\boldsymbol{x}$ and the node i, and r_i is the radius of the support domain Ω_i of the node i. If the node in the cell is located in the regular domain Ω_r, then the trial function matrix $[\Phi]$, the stiffness matrix $[K_r] + [K_r^*]$ and the loading vector $\{Q_r\} + \{Q_r^*\}$ can be computed in that order. If the node in the cell is located in the enriched domain Ω_s, then the enriched

trial function matrix $[\Psi]$, the stiffness matrix $[K_s]+[K_s^*]$ and the loading vector $\{Q_s\}+\{Q_s^*\}$ need be calculated additionally. Finally, the system of simultaneous algebraic equations as shown by Eqn (8) are assembled and the vector of all nodal displacement $\{q\}$ in the structure and the vector of three-dimensional stress intensity factors $\{K\}$ on the crack front can be calculated directly.

5 Results And Discussions

The accuracy and applicability of the enriched EFGM technique developed herein are demonstrated by solving several representative three-dimensional fracture problems. The discussed cracks include single-edge crack, embedded elliptical and semi-elliptical surface cracks, and quarter-elliptical corner crack, etc. For comparison, the Young's modulus of all structures is taken as $3.0\times10^7 psi$, and the Poisson's ratio of the single-edge crack is 0.33, while the Poisson's ratio of other types of cracks is taken as 0.3. Gauss quadrature is used to perform the numerical integration for each cell. $6\times6\times6$ integration points are selected for single-edge crack. For other types of cracks, however, $8\times8\times8$ integration points are adopted.

5.1 Single-edge crack

Figure 4 presents a thick plate with a single-edge through-thickness crack subjected to a uniform tension at both ends. The dimensions of the plate and the crack with slanted angle β are $W\times L\times H$ and a, respectively. The related geometric parameters are $a/W=0.5$, $L/W=1.75$ and $H/W=1.5$. Depending on the slanted angle $\beta=0^\circ$ or $\beta\neq0^\circ$, due to symmetry, only one quarter or one half of the thick plate need be analyzed using 207 nodes or 378 nodes, respectively.

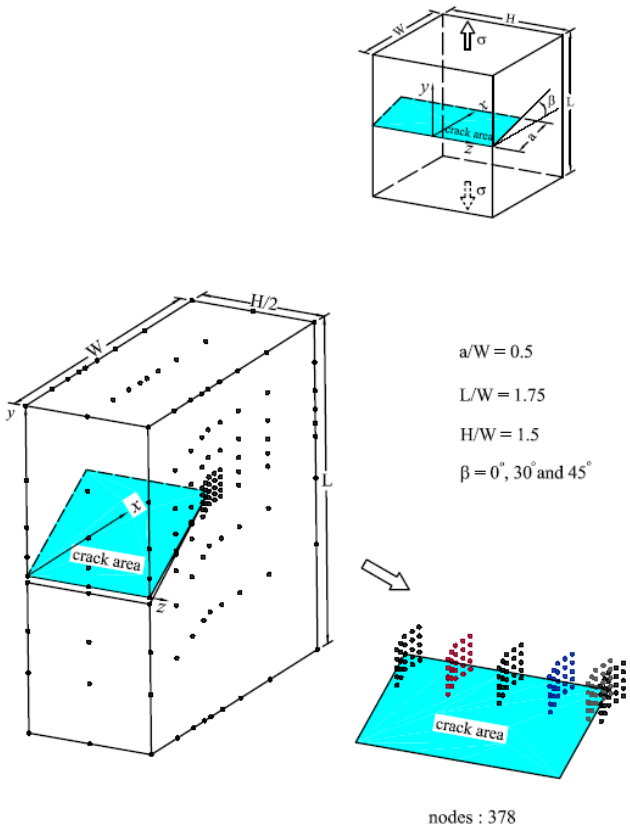

Figure 4 : The meshless model of a thick plate with a single-edge crack

Figure 5 plots the variation of the normalized mode-I stress intensity factors across the thickness of the single-edge crack ($\beta=0^\circ$). The normalized mode-I stress intensity factor is maximum at the midplane, and is about 1.39 % lower than that obtained from the plane strain solution. In addition, the present computed mode-I normalized stress intensity factor continues to decrease gradually and falls rapidly to about 0.20 at the free surface of the thick plate due to the boundary layer effect as compared with the zero value predicted by an approximate three-dimensional theory of plate (Hartranft and Sih, 1970) for a central crack in an infinite thick plate. For comparisons, the solutions of the finite element method/nodal force method (Raju and Newman, 1977) and the coupled finite element method/EFGM (Sukumar et al., 1997) are also shown in Fig. 5. It is worthwhile to note that the methods adopted by Raju and Newman (1977) and Sukumar et al. (1997) cannot accurately describe the boundary layer effect occurred at the free surface of the thick plate. Furthermore, the normalized mode-II and III stress intensity factors calculated herein are $10^{-4}\sim10^{-5}$ and therefore can be ignored in the analysis.

Figure 6 shows the variation of the normalized mode-I stress intensity factors at the midplane and free surface of the thick plate with a single-edge crack for various crack sizes a/W and slanted angles β. The maximum difference between the present computed normalized mode-I stress intensity factors at the midplane of the thick plate and those obtained from the plane strain solutions (Bowie, 1973) is about 4.1%. The normalized mode-I stress intensity factors at the free surface of the thick

plate are substantially lower than those of plane strain solutions. Additionally, as the crack size increases, the normalized mode-I stress intensity factors also increase. However, as the slanted angle β increases, the normalized mode-I stress intensity factors decline and make the fracture more difficult.

Figure 7 displays the variation of the normalized mode-II stress intensity factors of the single-edge crack at the midplane and the free surface of the thick plate for various crack sizes a/W and slanted angles β. At the midplane of the thick plate, the maximum difference between the mode-II normalized stress intensity factors and the plane strain solutions of Bowie (1973) is 3.7%. Importantly, when the slant angle $\beta = 0^\circ$, the loading σ is perpendicular to the crack a and the normalized mode-II stress intensity factors vanish. When the slant angle is $\beta = 30^\circ$ or 45°, the normalized mode-II stress intensity factors increase with the crack size a/W. However, when $a/W > 0.5$, the normalized mode-II stress intensity factors for the slant angle $\beta = 30^\circ$ exceed those for $\beta = 45^\circ$ due to the interaction of the crack front and the boundary. Again, the negligible normalized mode-III stress intensity factors calculated herein are about $10^{-4} \sim 10^{-5}$.

5.2 Embedded elliptical surface crack

As shown in Fig. 8(a), the geometric dimensions of the structure with the embedded elliptical surface crack are $2L \times 2L \times 2L$, and the major-axis and minor-axis lengths of the elliptical crack are $2c$ and $2a$. The cases for the structure with a semi-elliptical surface crack and a quarter-elliptical corner crack are displayed in Fig. 8(b) and 8(c), respectively. As an example, the meshless model with 448 nodes for the case of the quarter-elliptical corner crack is drawn in Fig. 8(d). Due to symmetry, only a half of the structure is considered in the analysis.

Figure 9 presents the variation of the normalized mode-I stress intensity factors k^{I}/k_{cir} for an embedded elliptical surface crack when $c/a = 1.0$, 2.0 and 4.0. $k_{cir}(= \frac{2}{\pi}\sigma\sqrt{\pi a})$ is the analytic solution for an infinite body with a penny-shaped crack of radius a (Sneddon, 1946). For the case of $c/a = 1.0$, since the object of the analysis herein is a finite body, the present computed normalized mode-I stress intensity factors are approximately 2.9% higher than the analytic solution derived for an elliptical surface crack embedded in an infinite body by Irwin (1962) as expected. When $c/a = 2.0$ or 4.0, the normalized mode-I stress intensity factors on the major axis ($\varphi = 0^\circ$) are minimum, and those on the minor axis ($\varphi = 90^\circ$) are maximum. As compared with the above analytic solutions, the maximum differences at these locations are 2.9% and 3.8%, respectively. The normalized mode-II and III stress intensity factors calculated herein are both about $10^{-4} \sim 10^{-5}$.

5.3 Semi-elliptical surface crack

Figure 10 displays the variation of the normalized mode-I stress intensity factor $k^{\mathrm{I}}/\frac{\sigma\sqrt{\pi a}}{\mathrm{E}(\varphi)}$ for the semi-elliptical surface crack for the cases of $c/a = 1.0$, 2.0 and 4.0. $\mathrm{E}(\varphi)$ is the elliptic integral of the second kind. As compared with those referenced solutions obtained using the finite element method / nodal force method (Raju and Newman, 1979), the maximum differences are 3.3%, 3.5% and 3.2%, respectively.

Since the boundary layer effect at the intersection between the crack front and the free surface of the structure was not taken into account in Raju and Newman (1979), the maximum differences between the normalized mode-I stress intensity factors calculated herein and the referenced solutions are evident at the location $\varphi = 0^\circ$ and $\varphi = 180^\circ$. However, when the semi-elliptical surface crack becomes narrow ($c/a = 4.0$), the boundary layer effect nearly vanishes.

5.4 Quarter-elliptical corner crack

Figure 11 describes the variation of the normalized mode-I stress intensity factors $k^{\mathrm{I}}/\frac{\sigma\sqrt{\pi a}}{\mathrm{E}(\varphi)}$ for the quarter-elliptical corner crack when $c/a = 1.0$, 2.0 and 4.0. As compared with the referenced solutions in the literature (Newman and Raju, 1983), the maximum differences are 5.0%, 4.5% and 5.6%, respectively. The distinct boundary layer effect at the intersections between the crack front and free surfaces ($\varphi = 0^\circ$ and $\varphi = 90^\circ$) can be viewed.

6 Concluding Remarks

An enriched element-free Galerkin method (EFGM) has been successfully developed to deal with three-dimensional fracture problems by incorporating the singularity behavior of the stress field near the crack front and the boundary layer effect at the intersection between the crack front and the free surface of the structure. By applying the enriched trial functions developed, the three-dimensional stress intensity factors are treated as

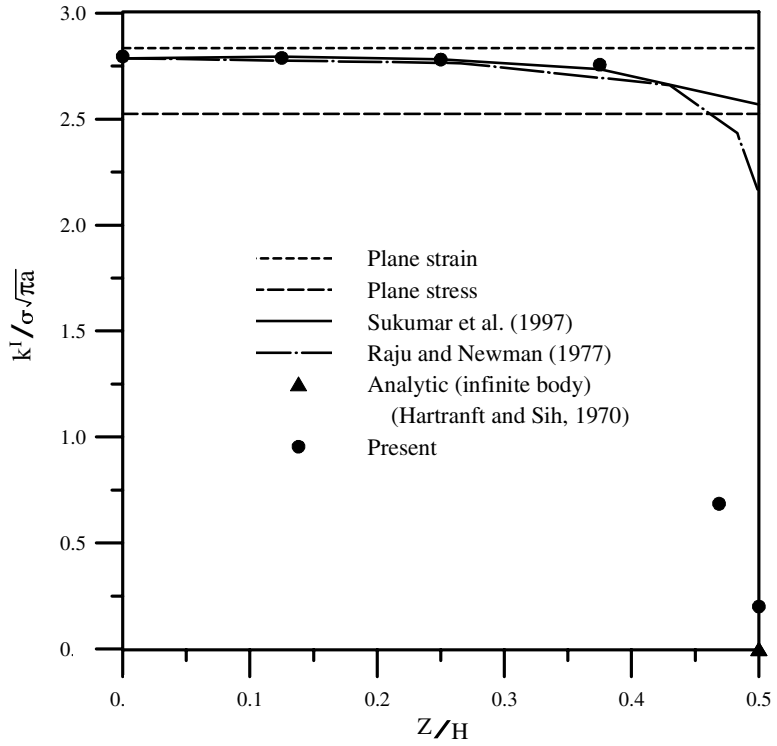

Figure 5 : The variation of the normalized mode-I stress intensity factors across the thickness of the single-edge crack ($\beta = 0^\circ$)

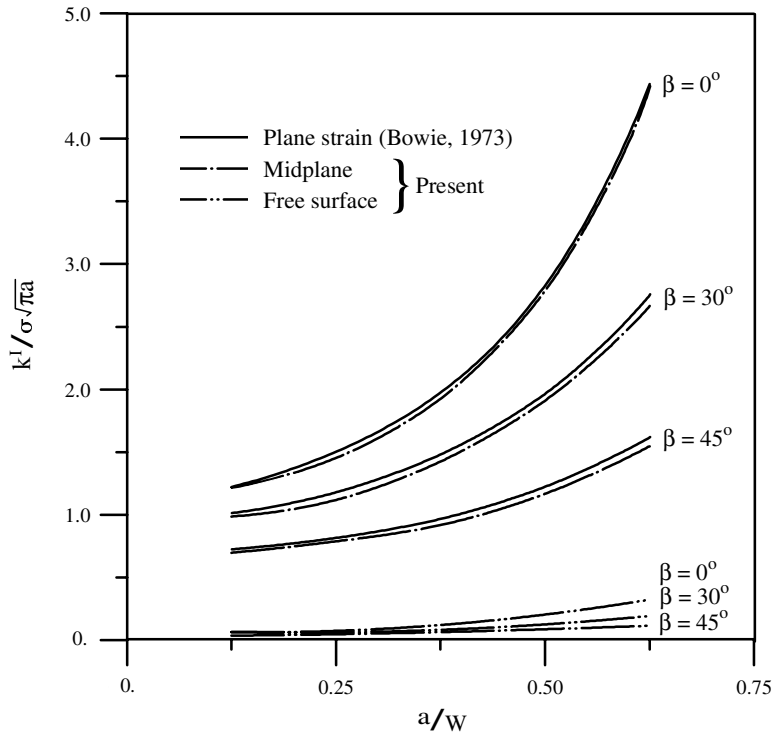

Figure 6 : The variation of the normalized mode-I stress intensity factors of the single-edge crack versus various crack sizes and slanted angles

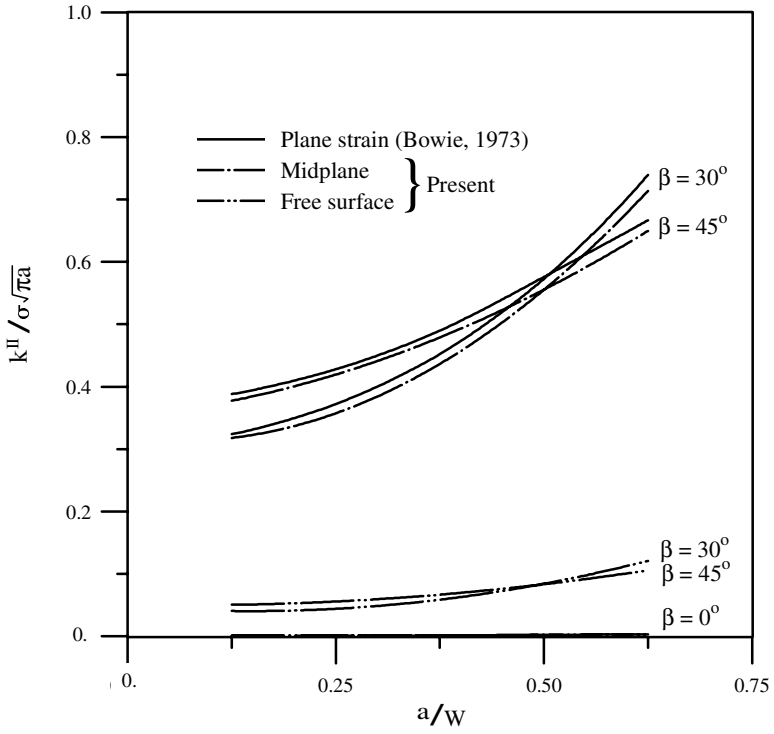

Figure 7 : The variation of the normalized mode-II stress intensity factors of the single-edge crack versus various crack sizes and slanted angles

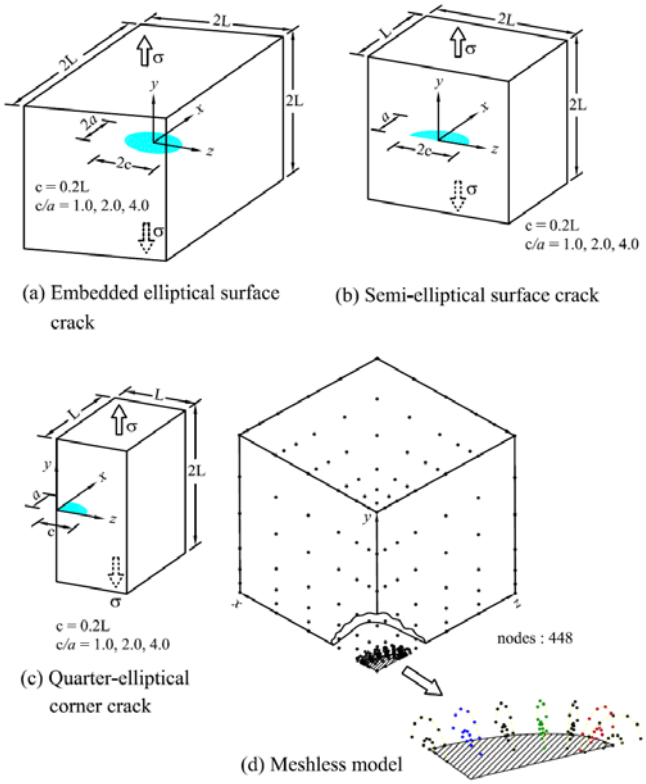

Figure 8 : The structure with various elliptical-shaped surface cracks

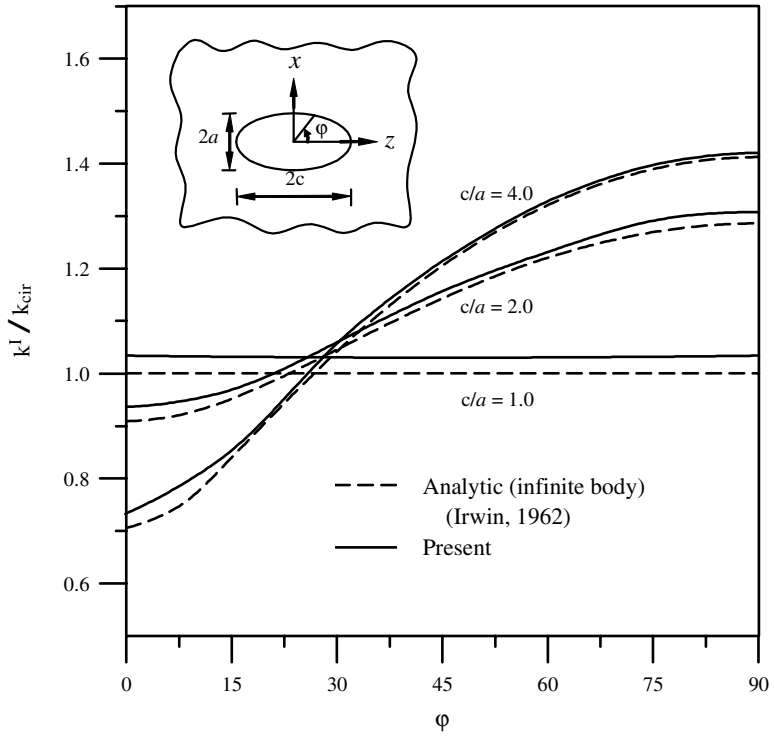

Figure 9 : The variation of the normalized mode-I stress intensity factors of the embedded elliptical surface crack along the crack front

undetermined parameters and can be computed with the nodal displacements directly and accurately. As a result, those factors that may influence the determination of stress intensity factors significantly, such as the crack size, the location of crack front and the boundary layer effect can be studied in details.

To further investigate practical three-dimensional fracture problems by the enriched EFGM developed, some future works should be probed. For example, a systematic and efficient means for selecting appropriate number of nodes in the sub-domain Ω_x needs to be established (Chen et al., 2001). That will affect the computational accuracy greatly. Besides, a further extension to explore the three-dimensional crack propagation problem for elastic or elastoplastic material is recommended.

Acknowledgement: The authors would like to thank the National Science Council of the Republic of China for financially supporting this research under Contract NSC-92-2212-E-007-059 and NSC 93-2212-E-007-017.

Appendix A: Displacement Field Nearby The Crack Front

As seen in Fig. 2, the linear elastic stress field around the point P near the crack front behaves a singular behavior $r^{-\frac{1}{2}}$ (Williams, 1957). r is the radial distance from the crack front to the point P on the $n-b$ plane; $t-n-b$ denote the local coordinate system with the origin at node j on the crack front. (t,n,b) represent the coordinates in tangent, normal and binormal directions, respectively. In addition, a boundary layer effect is found at the intersection point between the crack front and the free surface of the structure for an infinite plate with a central through-thickness crack (Folias, 1975). That is, the stress field is proportional to a singularity $r^{-(\frac{1}{2}+2\nu)}$ while the displacement field is proportional to $r^{\frac{1}{2}-2\nu}$. ν is the Poisson's ratio. To elucidate the boundary layer effect, after neglecting the effect of higher order terms, the three-dimensional global displacement components $u^{\alpha}(\alpha=1,2,3)$ at point P near node j on the crack front can be written as

$$u^{\alpha}=\sum_{j=1}^{n_c}\sum_{k=\mathrm{I}}^{\mathrm{III}}\sum_{\beta=\mathrm{I}}^{\mathrm{III}} t^{\alpha}_{\beta j} d^{\beta}_{kj} k^{k}_{j}.$$

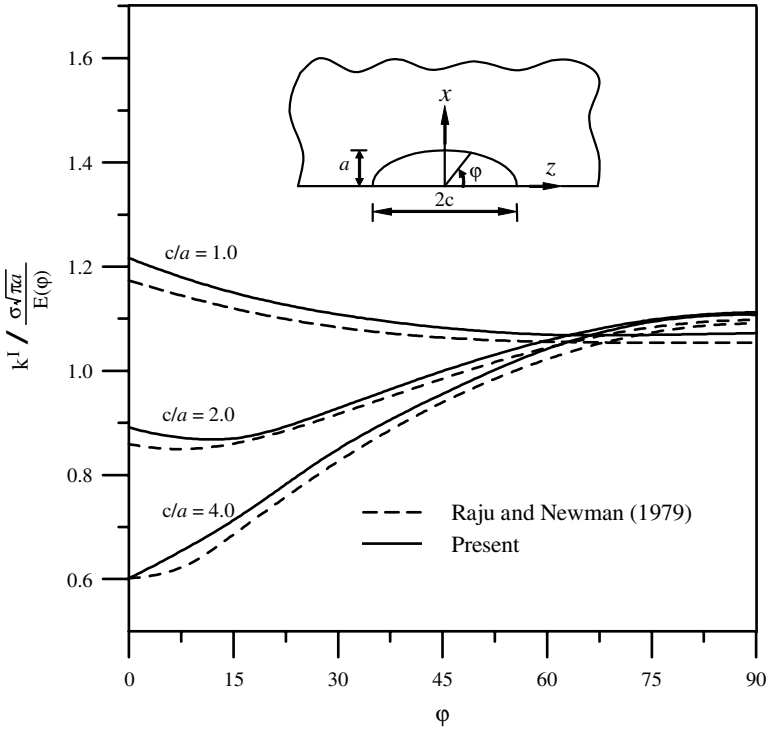

Figure 10 : The variation of the normalized mode-I stress intensity factors of the semi-elliptical surface crack along the crack front

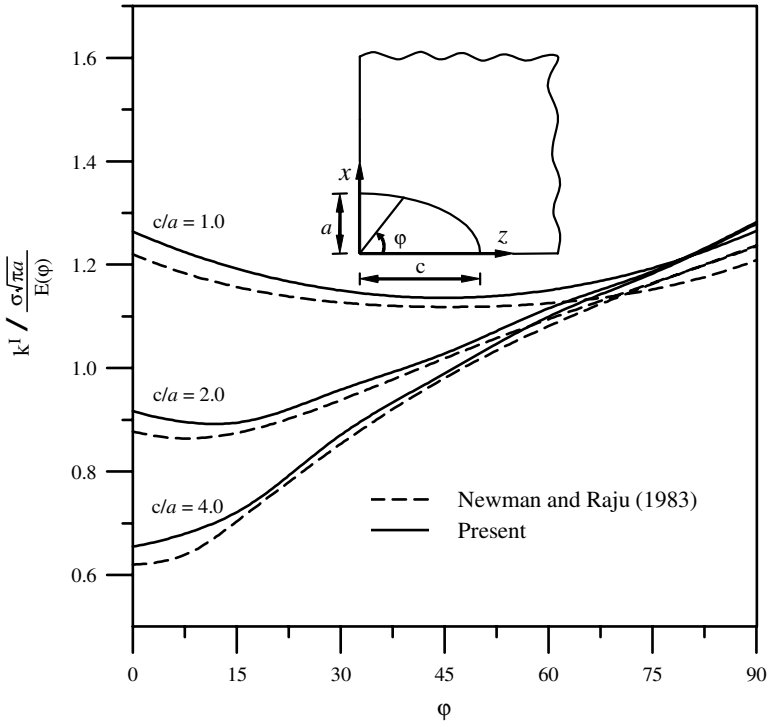

Figure 11 : The variation of the normalized mode-I stress intensity factors of the quarter-elliptical corner crack along the crack front

In matrix form

$$\left\{ \begin{array}{c} u^1 \\ u^2 \\ u^3 \end{array} \right\} = [T]\,[D] \left\{ \begin{array}{c} k_j^{\mathrm{I}} \\ k_j^{\mathrm{II}} \\ k_j^{\mathrm{III}} \end{array} \right\} \quad ,$$

The matrices $[T]$ and $[D]$ can be derived as

$$[T] = \left[\begin{array}{ccc} 0 & \cos\omega & -\sin\omega \\ 0 & \sin\omega & \cos\omega \\ 1 & 0 & 0 \end{array} \right]$$

and

$$[D] = \frac{1}{2\mu}\sqrt{\frac{2r}{\pi}} r^{-2\nu} \left[\begin{array}{cc} 0 & \\ \cos\frac{\theta}{2}(1-2\nu+\sin^2\frac{\theta}{2}) & \\ \sin\frac{\theta}{2}(2-2\nu-\cos^2\frac{\theta}{2}) & \\ 0 & 2\sin\frac{\theta}{2} \\ \sin\frac{\theta}{2}(2-2\nu+\cos^2\frac{\theta}{2}) & 0 \\ -\cos\frac{\theta}{2}(1-2\nu-\sin^2\frac{\theta}{2}) & 0 \end{array} \right],$$

where ω is the angle between the z-axis of the global coordinates $x-y-z$ and the t-axis of the local coordinates $t-n-b$ on the $x-z$ (or $n-t$) plane, as indicated in Fig. 2. μ is the shear modulus, and (r,θ) is the local polar coordinates of the point P on the $n-b$ plane.

References

Atluri, S. N. (2004a): The meshless method (MLPG) for domain & BIE discretizations, 680 pages, Tech Science Press.

Atluri, S. N. (2005): Applications of DTALE: damage tolerance analysis & life enhancement [3-D Non-planar Crack Growth], SID: STRUCTURAL INTEGRITY & DURABILITY, vol. 1, no.1, pp. 1-20.

Atluri, S. N., Han, Z. D. and Rajendran, A. M. (2004b): A new implementation of the meshless finite volume method, through the MLPG "Mixed" approach, *CMES: Computer Modeling in Engineering & Sciences*, vol. 6, no. 6, pp. 491-513.

Atluri, S. N., Han, Z. D. and Shen, S. (2003): Meshless local Petrov-Galerkin (MLPG) approaches for solving the weakly-singular traction & displacement boundary integral equations, *CMES: Computer Modeling in Engineering & Sciences*, vol. 4, pp. 507-518.

Atluri, S. N. and Kathiresan, K. (1979): 3-D analysis of surface flaws in thick-walled reactor pressure vessels using a displacement hybrid finite element method, *Nuclear Engineering and Design*, vol. 51, pp. 163-176.

Atluri, S. N., Kim, H. G. and Cho, J. Y. (1999): A critical assessment of the truly Meshless Local Petrov-Galerkin (MLPG), and Local Boundary Integral Equation (LBIE) methods, *Computational Mechanics*, vol. 24, pp. 348-372.

Atluri, S. N., Kobayashi, A. S. and Nakagaki, M. (1975): An assumed displacement hybrid finite element model for linear fracture mechanics, *International Journal of Fracture*, vol. 11, pp. 257-271.

Atluri, S. N. and Shen, S. (2002): The meshless local Petrov-Galerkin (MLPG) method, Tech Science Press.

Barsoum, R. S. (1976): On the use of isoparametric finite elements in linear fracture mechanics, *International Journal of Numerical Methods in Engineering*, vol. 10, pp. 25-37.

Belytschko, T., Lu, Y. Y. and Gu, L. (1994): Element-free Galerkin method, *International Journal for Numerical Methods in Engineering*, vol. 37, pp. 229-256.

Bowie, O. L. (1973): Solutions of plane crack problems by mapping technique, Mechanics of Fracture, (Ed. by Sih, G. C.), vol. 1, pp. 1-55, Noordhoff International Publ., Leyden.

Chen , W. H. and Chen, P. Y. (1984): Hybrid-displacement finite element model for the bending analysis of thin cracked plate, *International Journal of Fracture*, vol. 24, pp. 83-106.

Chen, W. H. and Guo, X. M. (2001): Element-free Galerkin method for three-dimensional structural analysis, *CMES: Computer Modeling in Engineering & Sciences*, vol. 2, pp. 497-508.

Ching, H. K. and Batra, R. C. (2001): Determination of crack tip fields in linear elastostatics by the meshless local Petrov-Galerkin (MLPG) method, *CMES: Computer Modeling in Engineering & Sciences*, vol. 2, pp. 273-289.

Fleming, M., Chu, Y. A. and Belytschko, T. (1997): Enriched element-free Galerkin methods for crack tip fields, *International Journal for Numerical Methods in Engineering*, vol. 40, pp. 1483-1504.

Folias, E. S. (1975): On the three-dimensional theory of cracked plates, *Transactions of the ASME, Series E : Journal of Applied Mechanics*, vol. 42, pp. 663-674.

Fung, Y. C. (1965): Foundations of solid mechanics,

Prentice-Hall.

Han, Z. D. and Atluri, S. N. (2002): SGBEM (for cracked local subdomain) FEM (for uncracked global structure) alternating method for analyzing 3D surface cracks and their fatigue growth, *CMES: Computer Modeling in Engineering & Sciences*, vol. 3, no. 6, pp. 699-716.

Han, Z. D. and Atluri, S. N. (2004): Meshless local Petrov-Galerkin (MLPG) approaches for solving 3D problems in elasto-statics, *CMES: Computer Modeling in Engineering & Sciences*, vol. 6, no. 2, pp. 169-188.

Hartranft, R. J. and Sih, G. C. (1970): An approximate three-dimensional theory of plates with application to crack problems, *International Journal of Engineering Science*, vol. 8, pp. 711-729.

Irwin, G. R. (1962): Crack-extension force for a part-through crack in a plate, *Transactions of the ASME, Series E : Journal of Applied Mechanics*, vol. 29, pp. 651-654.

Kaljević, I. and Saigal, S. (1997): An improved element free Galerkin method, *International Journal for Numerical Methods in Engineering*, vol. 40, pp. 2953-2974.

Kim, H. G. and Atluri, S. N. (2000): Arbitrary placement of secondary nodes, and error control in the meshless local Petrov-Galerkin (MLPG) method, *CMES: Computer Modeling in Engineering & Sciences*, vol. 1, pp.11-32.

Li, Q., Shen, S., Han, Z. D. and Atluri, S. N. (2003): Application of meshless Petrov-Galerkin (MLPG) to problems with singularities, and material discontinuities, in 3-D elasticity, *CMES: Computer Modeling in Engineering & Sciences*, vol. 4, pp. 571-586.

Lin, H and Atluri, S. N. (2000): Meshless local Petrov-Galerkin (MLPG) method for convection-diffusion problems, *Computing Modeling in Engineering & Sciences*, vol. 1, pp.45-60.

Liu, Y. Y., Belyschko, T. and Gu, L. (1994): A new implementation of the element free Galerkin method, *CMES: Computer Methods in Applied Mechanics & Engineering*, vol. 113, pp. 397-414.

Newman, J. C., Jr. and Raju, I. S. (1981): An empirical stress-intensity factor equation for the surface crack, *Engineering Fracture Mechanics*, vol. 15, pp. 185-192.

Newman, J. C., Jr. and Raju, I. S. (1983): Stress-intensity factor equations for cracks in three-dimensional finite bodies, Fracture Mechanics, vol. I : Theory and Analysis, ASTM STP-791, Ed. by Lewis, J. C. and Sines, G., pp. I238-I265.

Organ, D., Fleming, M., Terry, T. and Belytschko, T. (1996): Continuous meshless approximations for non-convex bodies by diffraction and transparency, *Computational Mechanics*, vol. 18, pp. 225-235.

Raju, I. S. and Newman, J. C., Jr. (1977): Three dimensional finite-element analysis of finite-thickness fracture specimens, NASA-TN-D-8414.

Raju, I. S. and Newman, J. C., Jr. (1979): Stress-intensity factors for a wide range of semi-elliptical surface cracks in finite thickness plates, *Engineering Fracture Mechanics*, vol. 11, pp. 817-829.

Sneddon, I. N. (1946): The distribution of stress in the neighborhood of a crack in an elastic solid, *Proceedings of the Royal Society A*, vol. 187, pp. 229-260.

Sukumar, N., Moran, B. and Belytschko, T. (1997): An element-free Galerkin method for three-dimensional fracture mechanics, *Computational Mechanics*, vol. 20, pp. 170-175.

Williams, M. L. (1957): On the stress distribution at the base of a stationary crack, *Transactions of the ASME, Series E : Journal of Applied Mechanics*, vol. 24, pp. 109-114.

Zhu, T. and Atluri, S. N. (1998): A modified collocation method and a penalty formulation for enforcing the essential boundary conditions in the element free Galerkin method, *Computational Mechanics*, vol. 21, pp. 211-222.